Ex-situ modification of lattice thermal transport through coherent and incoherent heat baths

Tengfei Ma, Yan Wang

PII: S2542-5293(22)00282-6

DOI: https://doi.org/10.1016/j.mtphys.2022.100884

Reference: MTPHYS 100884

To appear in: Materials Today Physics

Received Date: 13 July 2022

Revised Date: 17 September 2022

Accepted Date: 6 October 2022

Please cite this article as: T. Ma, Y. Wang, Ex-situ modification of lattice thermal transport through coherent and incoherent heat baths, *Materials Today Physics*, https://doi.org/10.1016/j.mtphys.2022.100884.

This is a PDF file of an article that has undergone enhancements after acceptance, such as the addition of a cover page and metadata, and formatting for readability, but it is not yet the definitive version of record. This version will undergo additional copyediting, typesetting and review before it is published in its final form, but we are providing this version to give early visibility of the article. Please note that, during the production process, errors may be discovered which could affect the content, and all legal disclaimers that apply to the journal pertain.

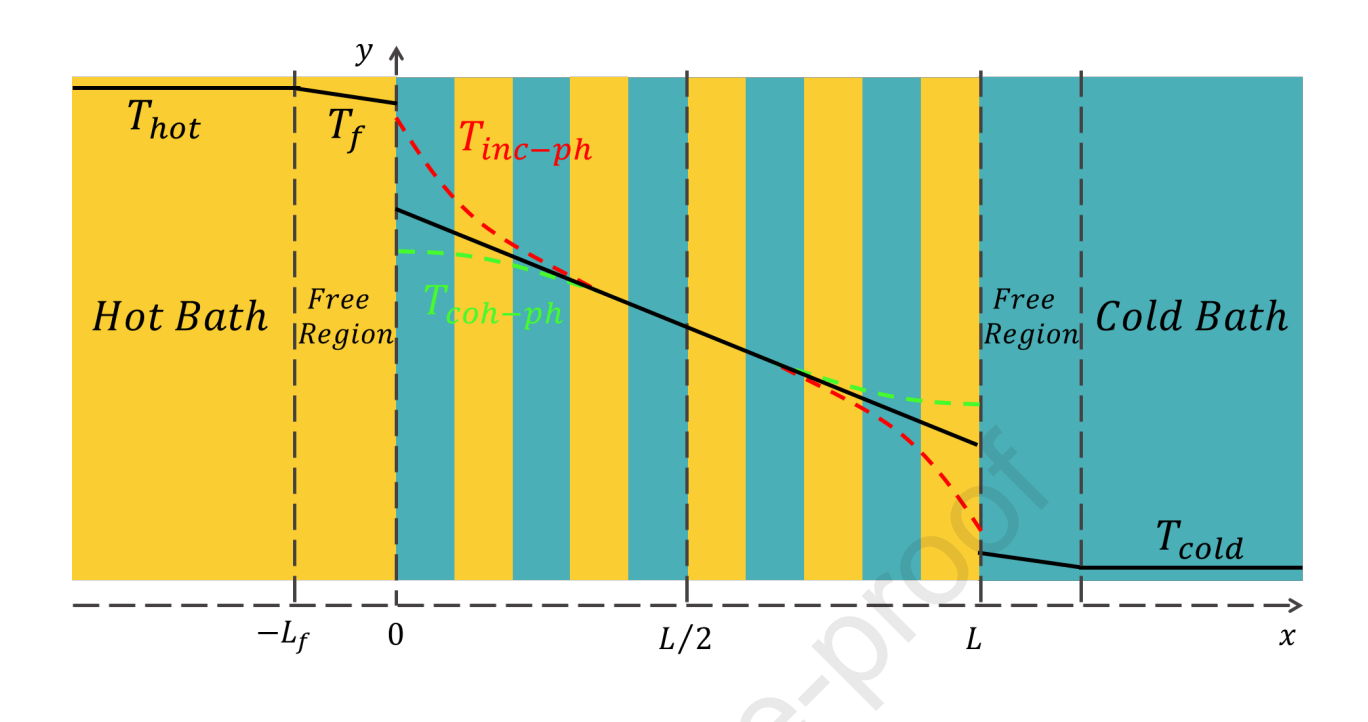
© 2022 Elsevier Ltd. All rights reserved.



# Credit author statement

Tengfei Ma: Conceptualization, Formal analysis, Software, Writing - Original Draft, Writing - Review and Editing.

Yan Wang: Conceptualization, Formal analysis, Supervision, Writing - Original Draft, Writing - Review and Editing.



# Ex-situ modification of lattice thermal transport through coherent and incoherent heat baths

Tengfei Maa, Yan Wanga,\*

<sup>a</sup>Department of Mechanical Engineering, University of Nevada, Reno, Nevada 89557, USA.

#### **Abstract**

Most of the current strategies for tailoring the thermal conductivity of materials directly modify the composition or structure of a material, for instance, by alloying or modifying the microstructure. In this work, we demonstrate the ex-situ modification of thermal conductivity of devices containing secondary periodicity through the rational choice of heat baths. Molecular dynamics simulations show that coherent baths, of which the phonon transmission spectrum matches with that of the device, can greatly increase the thermal conductivity of Lennard-Jones (up to 400%) and silicon/germanium (up to 40%) superlattice devices, when compared with the cases of incoherent baths. Phonon transmission calculations reveal strong coherent-incoherent phonon nonequilibrium near the interface between the device and incoherent baths, which, as elucidated by a proposed coherent-incoherent phonon transport model, hinders thermal transport. This work provides a strategy to greatly tailor the thermal conductivity of nanodevices ex-situ without the need to irreversibly modify the structure or composition of the device.

Keywords: phonon transport, coherent phonons, superlattice, molecular dynamics

#### 1. Introduction

Many thermal engineering strategies so far were derived from the materials science perspective. One historically effective but highly unpredictable route is through the discovery of new materials, for example, the groundbreaking lab-fabrication of graphene [1] and other two-dimensional materials that have various exotic thermal transport properties [2, 3, 4, 5], the recent report of boron arsenide [6, 7, 8, 9] and cubic boron nitride [10, 11] displaying high thermal conductivity comparable to that of diamond, and low thermal conductivity materials such as SnSe [12, 13, 14] for thermoelectric applications. The other much more widely attempted strategy is to modify the existing materials into various nanostructured or dirty materials, such as alloys [15], nanowires [16], thin films [17], phononic crystals [18, 19, 20, 21, 22], and hierachical structures [23, 24, 25, 26, 27]. More recently, the feasibility of using external fields, particularly electric field [28, 29, 30], to tune the thermal conductivity of materials has been investigated through first-principles calculations, even though significant efforts are expected for researchers to achieve this strategy experimentally. Nonetheless, the idea behind this strategy is inspiring: how can we engineer the thermal transport properties of materials ex situ?

Recently, there is a rising notion of the importance of nonequilibrium between heat carriers on the overall heat transfer characteristics in heterogeneous systems. For instance, electron-phonon nonequilibrium near metal-nonmetal interfaces was found to hinder thermal transport across the interface [31, 32, 33] and even the nonequilibrium among phonon modes can notably affect thermal transport across nonmetal-nonmetal interfaces [34, 35]. Even in homogeneous systems, the difference in the phonon distribution in the heat baths and device in nonequilibrium molecular dynamics simulations was found to cause notable nonequilibrium between phonons, altering the effective thermal conductivity displayed by the system. [36]

In our recent studies, we have found significant contribution of coherent phonons to heat conduction in Lennard-Jones superlattices [37, 38, 39, 40] and graphene-hexagonal boron nitride superlattices [21]. Similar coherent phonon heat

Email address: yanwang@unr.edu (Yan Wang)

<sup>\*</sup>Corresponding author

conduction behaviors were observed and confirmed on other systems, for example, silicon-germanium superlattice [41, 42]. "Coherent phonon" was historically used by many researchers to refer to the collective atomic movements induced by ultrafast lasers or that occur naturally during certain phase transformation processes. Differently, "coherent phonon" used in our work as well as many other research groups' publications [43] denote the phonon modes stemming from the new, large unit cell of the periodic structure, which are believed, but not yet confirmed, to arise from the interference between the back-scattered incoherent phonons (i.e., the modes corresponding to the primitive unit cell of the constituting material) at the periodically arranged interfaces [44, 45]. A unique behavior of coherent phonons as such is that they are not scattered at the interfaces, merely because interfaces are essentially part of the new large unit cell. As a result, coherent phonons can conduct a significant amount of heat along its path across multiple interfaces, which could otherwise scatter incoherent phonons greatly and lead to ultralow thermal conductivity [45, 38, 21]. Noting the dominant coherent phonon contribution to thermal transport in periodic structures—which widely exist in practical applications, e.g., periodically arranged nanotransitors [46, 47, 48, 49] and quantum cascade lasers [50, 51]—it is imperative to investigate how to engineer the nonequilibrium between coherent and incoherent phonons to tailor thermal transport properties over a wide range. Through this work, we will demonstrate the importance of this degree of freedom in heat carriers for engineering thermal transport properties ex situ.

#### 2. Methods

#### 2.1. Molecular Dynamics Simulation

We perform nonequilibrium molecular dynamics (NEMD) simulations to predict the lattice thermal conductivity of different superlattice systems, including conceptual Lennard-Jones (LJ) systems and more realistic silicon/germanium (Si/Ge) systems. For the LJ systems, the interactions between atoms are modeled by the LJ potential,

$$\phi_{ij}(r_{ij}) = 4\epsilon \left[ \left( \frac{r_0}{r_{ij}} \right)^{12} - \left( \frac{r_0}{r_{ij}} \right)^6 \right],\tag{1}$$

where  $\phi_{ij}$  is the potential energy between atoms i and j,  $r_{ij}$  is the distance between atoms i and j,  $\epsilon$  is the potential energy well depth that describes the bond strength, and  $r_0$  is the zero-crossing distance for the potential energy. One set of LJ systems has  $\epsilon = 0.1664 \ eV$  that corresponds to 16 times that of the value for solid argon ( $\epsilon_{Ar} = 0.0104 \ eV$ ) while the other has  $\epsilon = 32\epsilon_{Ar}$ . All the other setups are exactly the same for these two sets of LJ systems in our NEMD simulations. For the Si/Ge systems, the interatomic interactions are described by the Stillinger-Weber potential [52, 53, 54].

Fig. 1 shows two different heat bath structures studied in this work. In the first setup, the hot and cold baths are pure materials as shown in Fig. 1a. We will refer to this setup as "incoherent baths", because the phonon modes in those heat baths follow the dispersion relations of pure materials that differ from those of the superlattice device. In the other setup, the hot and cold baths are superlattices that are exactly the same as the superlattice device, as shown in Fig. 1b. We will refer to this setup as "coherent baths", because the phonon modes in the superlattice heat baths follow the same superlattice phonon dispersions as the device. Obviously, the coherent baths designed in this way represent the extreme case where the heat baths perfectly match with the device in phonon spectra.

The LAMMPS [55, 56] package is used for all the molecular dynamics simulations in this work. In our NEMD simulations, the system is first relaxed in the isothermalisobaric (NPT) ensemble at the target temperature and 0 Pa for 1.5 ns with the Nóse-Hoover thermostat [57]. Then NEMD simulations are performed by switching the system integration algorithm from NPT to the microcanonical ensemble (NVE) and maintain the hot bath and cold bath at different temperature. The atomic velocities in the hot and cold baths are rescaled at every time step using the simple velocity rescaling algorithm to maintain a constant temperature throughout the entire simulation. To alleviate or even eliminate possible artificial effects related to temperature control in the heat baths, we leave free regions that are one superlattice period thick, respectively, between the device and each heat bath, same as the setup of NEMD simulations in our previous studies [38]. The temperature difference  $\Delta T$  across the superlattice device is estimated by the difference between the average temperature of two free regions defined in Fig. 1. The heat current J flowing across the device can be readily obtained from LAMMPS. Finally, the effective thermal conductivity of the device can be calculated as

$$k_{eff} = G \cdot L = \frac{J \cdot L}{A_c \cdot \Delta T},\tag{2}$$

where G,  $A_c$ , and L are the thermal conductance, cross-sectional area, and length of the device, respectively.

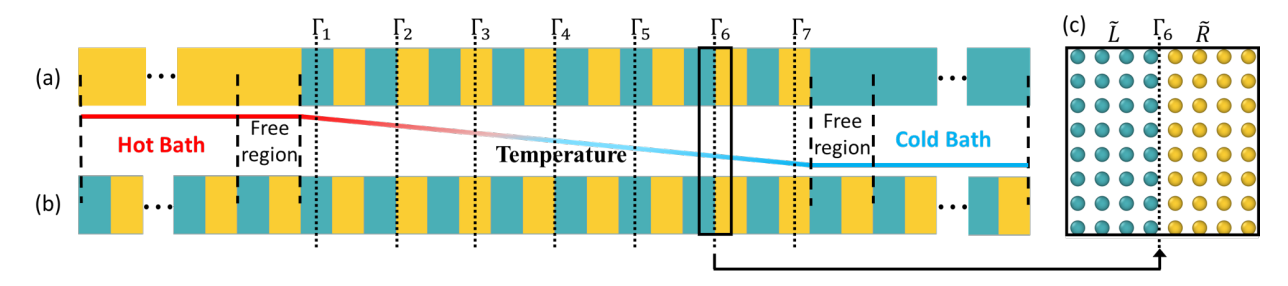


Figure 1: Schematic of the setup of NEMD simulations using (a) incoherent baths and (b) coherent baths.  $\Gamma_1, \Gamma_2, ...,$  and  $\Gamma_7$  denote seven interfaces at which phonon transmission spectra are measured. (c) Zoomed-in view of an interface region for measuring phonon transmission spectra  $\Gamma$ .  $\tilde{L}$  and  $\tilde{R}$  denote the left and right section of the interface region. The length of the heat bath is 8 periods of the corresponding superlattice structure.

#### 2.2. Phonon Transmission Calculation

In order to investigate the phonon transmission and coherent-incoherent phonon nonequilibrium in our model systems, we spectrally decompose the heat flux obtained in our NEMD simulations to calculate the phonon transmission using [58, 59]

$$Q(\omega) = \sum_{i \in L} \sum_{j \in R} \left( -\frac{2}{t_{simu}\omega} \sum_{\alpha,\beta} Im \langle \hat{v}_i^{\alpha}(\omega)^* K_{ij}^{\alpha\beta} \hat{v}_j^{\beta}(\omega) \rangle \right), \tag{3}$$

where  $Q(\omega)$  is the spectral heat current,  $\omega$  is the frequency, i and j are respectively the atom indices in the left  $(\tilde{L})$  and right  $(\tilde{R})$  part of a selected cross section (as shown in Fig. 1c),  $t_{simu}$  is the total NEMD simulation time,  $\alpha$  and  $\beta$  are Cartesian coordinates,  $\hat{v}$  is the Fourier transform of atom velocity and \* denotes the conjugate operator, and  $K_{ij}^{\alpha\beta}$  is the force constant matrix. From the decomposed spectral heat current, the spectral phonon transmission function  $\Gamma(\omega)$  is calculated as [59]

$$\Gamma(\omega) = \frac{Q(\omega)}{k_b \Delta T} \tag{4}$$

where  $k_b$  is the Boltzmann constant and  $\Delta T$  is the temperature bias between the hot and cold bath in the NEMD simulations. The velocity trajectories of 25 million steps are sampled from our NEMD simulations to calculate the spectral phonon transmission. In order to investigate how the phonon transmission spectra change along the device, we select seven locations along the cross-plane direction of the device and measure the phonon transmission spectra at those cross-sections, as schematically illustrated in Fig. 1.

#### 3. Results and discussions

To begin with, we compare between the case when the superlattice device is sandwiched between two incoherent baths (Fig. 1a) and the case with two coherent baths (Fig. 1b). To draw a more general conclusion, we study both conceptual Lennard-Jones (LJ) systems and more realistic Si/Ge systems.

Fig. 2a-f display the thermal conductivity of the device, sandwiched between either coherent baths or incoherent ones, as a function of device length for different temperatures. Comparing between the thermal conductivity of devices with incoherent baths ( $\kappa_{eff,inc-bath}$ ) and that with coherent baths ( $\kappa_{eff,coh-bath}$ ) in each panel of Fig. 2a-f leads to the immediate conclusion that the use of coherent baths can significantly increase the thermal conductivity of the device. Notably, the increase can be as high as 400% for the LJ device with an average superlattice layer thickness of 2 UC, bond strength of  $32\epsilon_{Ar}$ , and at a low temperature of 30 K, as shown in Fig. 2g. In addition, Fig. 3a shows the thermal conductivity of Si/Ge superlattice devices obtained from our NEMD simulations. The device has an average layer thickness of 4 UCs of Si or Ge, which corresponds to an average period thickness of 2.22 nm. Obviously, the devices with coherent baths demonstrate notably higher thermal conductivity than those with incoherent baths, agreeing with our observations on Lennard-Jones systems (Fig. 2). This directly confirms our hypothesis that the thermal conductivity of a superlattice device can be substantially modified even without modifying its structure or

composition. More importantly, the thermal conductivity of homogeneous systems can hardly depend on the type of heat baths as much as the superlattice devices studied in this work, suggesting the potential importance for exploiting this mechanism to better control thermal transport in devices containing periodically arranged nano-components, like the periodic semiconductor layers in a quantum cascade laser or the periodically arranged transistors in an integrated circuit.

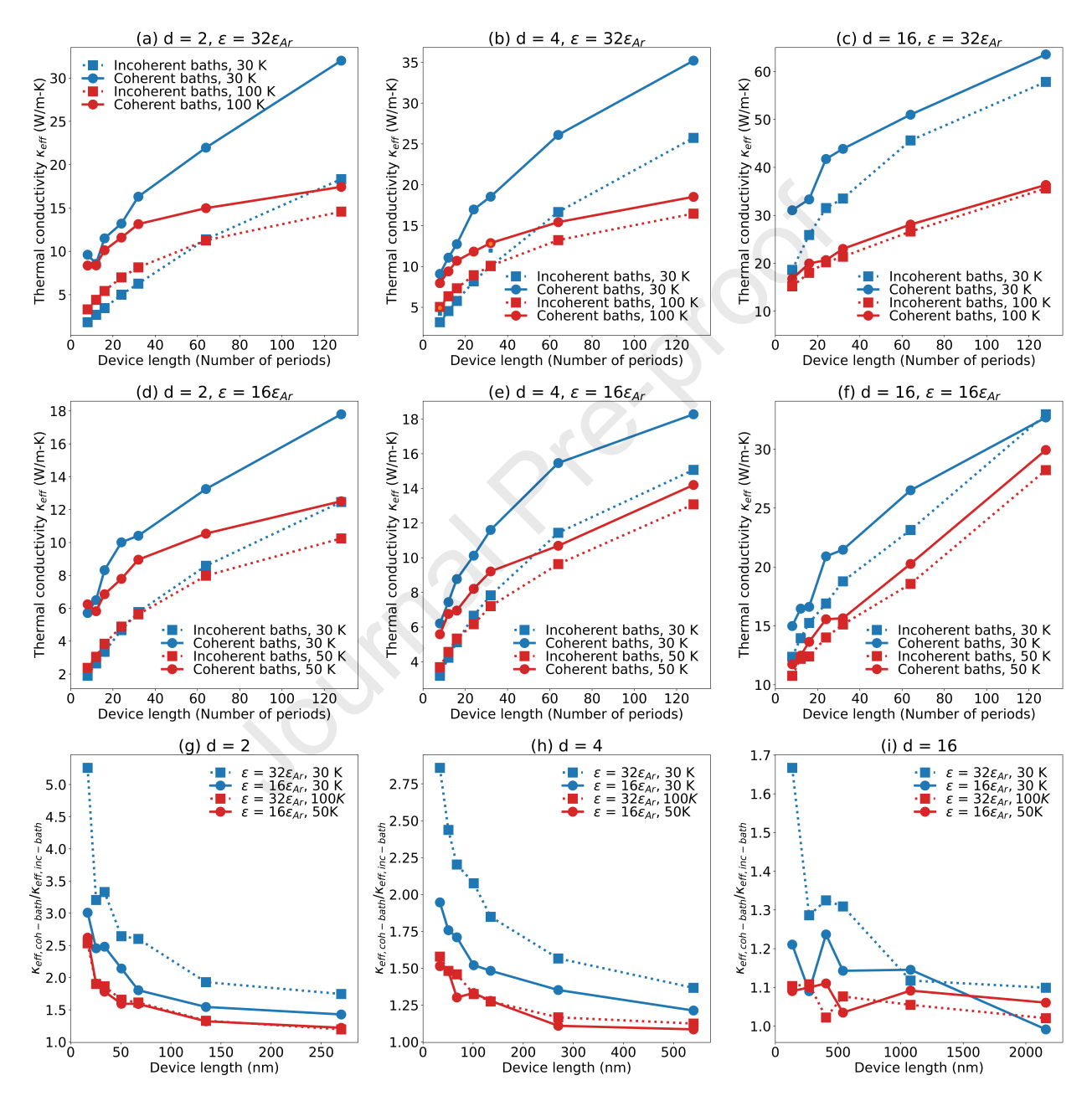


Figure 2: (a-f) Thermal conductivity of LJ superlattices with different layer thickness d and bond strength  $\epsilon$  at different temperatures. (g-i) Enhancement ratio of thermal conductivity by replacing incoherent baths with coherent baths for LJ superlattices.

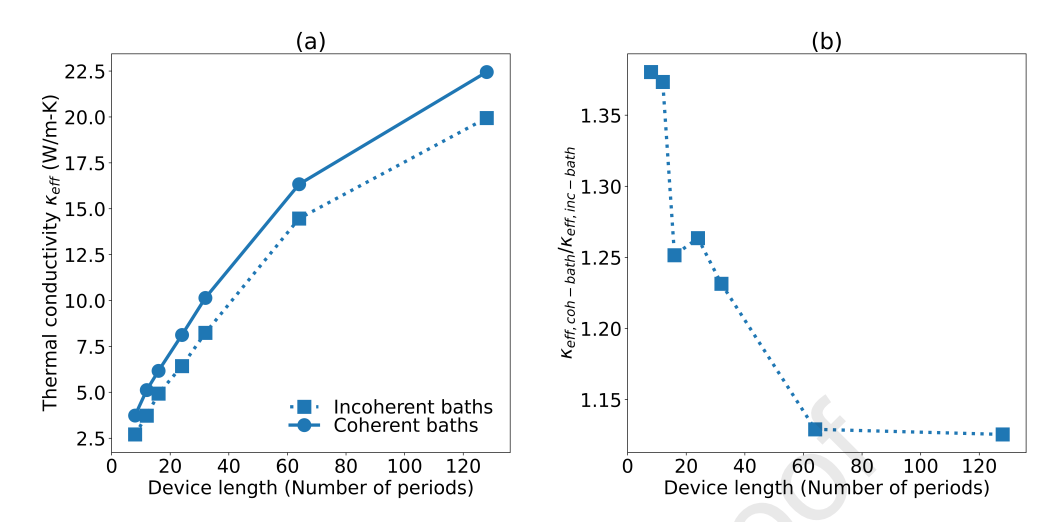


Figure 3: (a) Thermal conductivity of Si/Ge superlattices with different device length. (b) Enhancement ratio of thermal conductivity by replacing incoherent baths with coherent baths for Si/Ge superlattices.

To quantify how coherent baths can promote thermal transport in the device, we calculate the ratio of the effective thermal conductivity using coherent and incoherent baths as  $\kappa_{eff,coh-bath}/\kappa_{eff,inc-bath}$  and plot it in Fig. 2g-i and Fig. 3 for LJ systems and Si/Ge systems, respectively. As expected, the heat bath effect weakens as the device becomes longer, which directly results from the fact that regions farther away from the heat bath are affected less than those close to the baths. Nonetheless, despite the monotonic decrease in  $\kappa_{eff,coh-bath}/\kappa_{eff,inc-bath}$  as the device length increases, devices longer than 500 nm (e.g., the longest device in Fig. 2h is 540 nm long) can still have approximately 20-30% higher thermal conductivity when coherent baths are applied than the case with incoherent ones. This proves the robustness of the heat baths effect in nanosized devices.

It is worth noting that previous studies have revealed notable dependence of the effective thermal conductivity  $\kappa_{eff}$  on the thermostatting algorithms in molecular dynamics simulations. For instance, Feng et al. demonstrated that the Nóse-Hoover thermostat preferentially excites optical phonons, leading to different temperature profiles than those from NEMD simulations using the Langevin thermostats. [60] The dependence of temperature profile and  $\kappa_{eff}$  on thermostatting algorithm was further investigated in Ref. 36 and Ref. 61, but the reported variation in  $\kappa_{eff}$  was usually less than 10%. We have confirmed that thermostatting algorithms, though affecting the absolute values of  $\kappa_{eff}$  of the superlattice devices studied in this work, do not affect our conclusion—the choice between coherent bath and incoherent bath is a more significant factor affecting  $\kappa_{eff}$  of the superlattice device.

Comparing between the  $\kappa_{eff,coh-bath}/\kappa_{eff,inc-bath}$  curves for different temperatures in Fig. 2g-i indicates a strong temperature dependence of the heat bath effect. The reduced heat baths effect at higher temperature is presumably due to the enhanced anharmonic scattering of phonons that suppress the coherent phonon transport [39].

Furthermore, the comparison between Fig. 2a and Fig. 2d, between Fig. 2b and Fig. 2e, and between Fig. 2c and Fig. 2f, clearly demonstrates that the heat bath effect is more prominent for systems with a larger bond strength. The comparison among Fig. 2a-c and among Fig. 2d-f, which only differ in the period length of the superlattice device, indicates diminishing heat bath effects as the superlattice period becomes larger.

Before we proceed to perform detailed mode-wise phonon analysis to understand the above observations rigorously, we emphasize that the conditions that favor heat bath effect—lower temperature, shorter superlattice period, and stronger bond strength—all agree with the conditions at which coherent phonons are more dominant in thermal transport in superlattices, as derived from our previous studies [38, 37, 39]. In particular, in Ref. 38, we demonstrate through nonequilibrium molecular dynamics (NEMD) simulations and two-phonon decomposition analysis that coherent phonon contribution to heat conduction in sueprlattices increases at lower temperature, in superlattices with shorter period, and in superlattices with stronger bonds. This, as we will demonstrate later, is not a coincidence and the reason why such strong heat bath effect can emerge in superlattice devices is because coherent phonons can dominate heat conduction in these types of systems.

To quantify the fluctuation in spectral phonon transmission and thus phonon nonequilibrium, herein we define  $\Delta\Gamma_i(\omega)$ 

as the scaled deviation of local transmission spectrum ( $\Gamma_i(\omega)$ ) at different locations along the device ( $\Gamma_1, \Gamma_2, ..., \Gamma_7$  in Fig. 1) from the spectrum at the center of the device ( $\Gamma_4(\omega)$ ). Specifically,

$$\Delta\Gamma_i(\omega) = \frac{\Gamma_i(\omega) - \Gamma_4(\omega)}{\int_0^{\omega_{max}} \Gamma_4(\omega) d\omega}, \ i = 1, 2, 3, 5, 6, 7$$
 (5)

where  $\omega_{max}$  is the maximum phonon frequency.

In Fig. 4a-f, the shaded areas in each panel represent  $\Delta\Gamma_i(\omega)$  and are plotted against the left axis, while the blue curve represents  $\Gamma_4(\omega)$  and is plotted against the right axis. It is expected that the phonon transmission spectra should stay the same in a system with fully equilibrium phonons. In other words, any variation in the transmission spectrum at different locations indicates a net exchange of heat between phonon channels, i.e., a certain degree of phonon nonequilibrium, if the variation is more significant than the inherent noise of molecular dynamics simulations. Apparently, Fig. 4a-c demonstrate remarkable variation of phonon transmission spectra in the heat flow direction when incoherent baths are applied to the superlattice device, which indicates strong nonequilibrium among phonons. Such nonequilibrium among phonons, which will be demonstrated with an analytical model later, can directly hinder thermal transport, leading to reduced thermal conductivity of the device. In contrast, all the cases with coherent baths (Fig. 4d-f) show rather location-independent phonon transmission spectra, suggesting much less significant nonequilibrium between phonons than the case with incoherent baths.

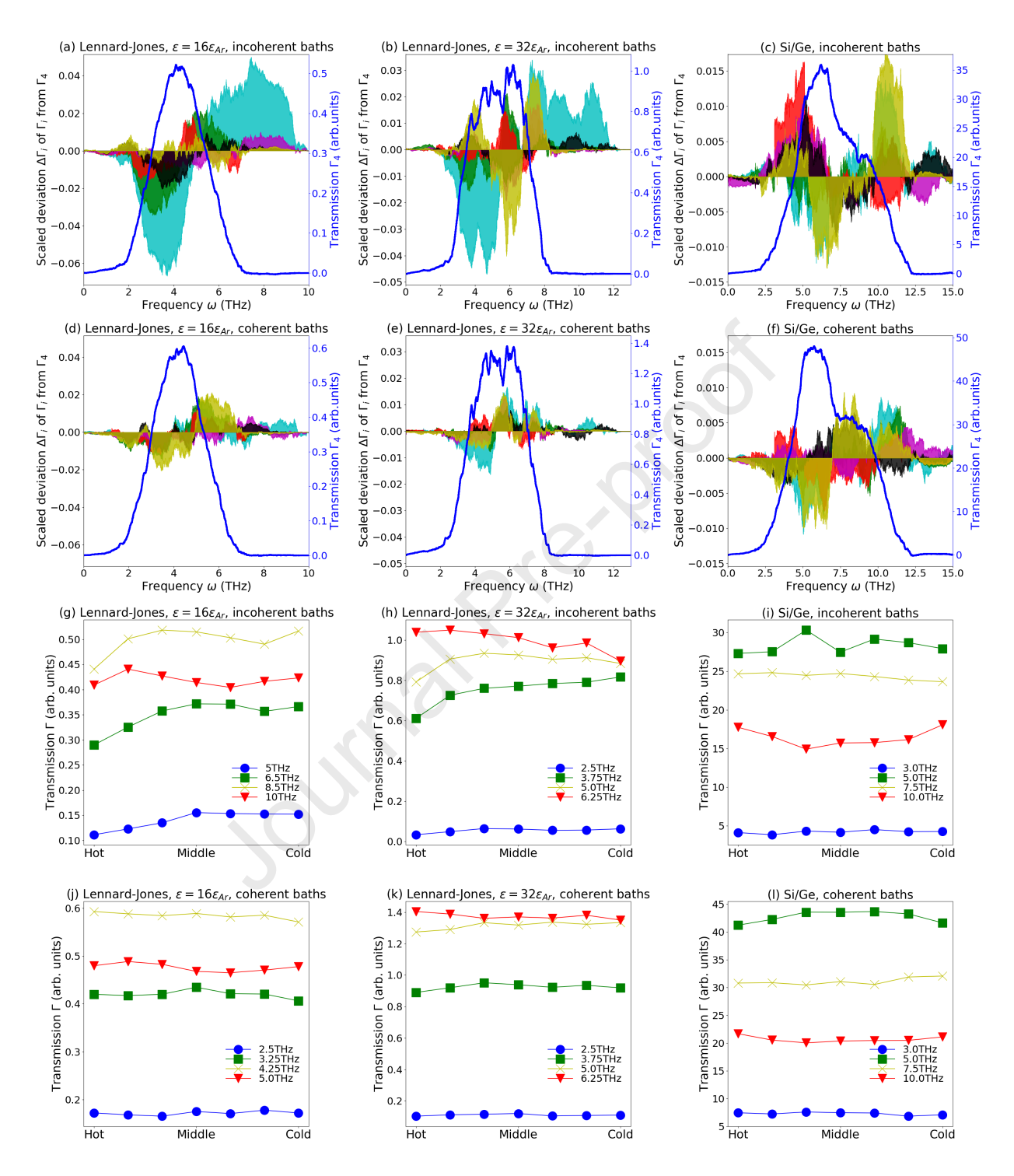


Figure 4: (a-f) Left axis (shaded areas): deviation of the phonon transmission spectrum  $\Gamma_i$  (location along device: i=1, 2, 3, 5, 6, and 7, as described in Figs. 1a and b) from  $\Gamma_4$ ; right axis (blue curve):  $\Gamma_4$ , i.e., phonon transmission spectrum at the center of the device. (g-l) Phonon transmission as a function of location along the device. *Hot* denotes the cross section close to the hot bath ( $\Gamma_1$ ) while *Cold* represents the cross section close to the cold bath ( $\Gamma_7$ ).

To demonstrate the nonequilibrium among phonons more clearly, we also plot the transmission function  $\Gamma$  for phonons

of specific frequencies as a function of location along the heat flow direction. As shown in Fig. 4g-i, the transmission function changes significantly on the path of heat flow from the hot bath to the cold bath, when the heat baths are incoherent to the device. In contrast, much less variation in phonon transmission spectra is observed when coherent baths are applied, as displayed in Fig. 4j-l.

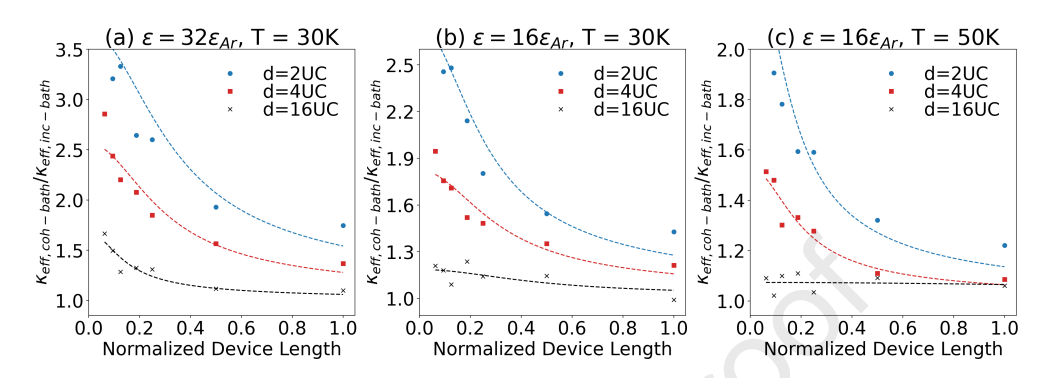


Figure 5: Schematic illustration of the proposed coherent-incoherent phonon transport model for the case when a superlattice device is sandwiched between two incoherent heat baths. The schematic also shows the nonequilibrium between coherent phonon and incoherent phonon near the interfaces between the incoherent heat baths and the device.

Finally, we propose a coherent-incoherent phonon transport model to analytically elucidate the effect of phonon nonequilibrium on the effective thermal conductivity  $\kappa_{eff}$  of the device, which can explain why coherent baths lead to a higher  $\kappa_{eff}$  than a system with incoherent baths.

Our model follows the idea of the phenomenological two-temperature model, which has successfully described electron-phonon nonequilibrium near interfaces between nonmetallic and metallic materials and predict the resulting thermal resistances [32, 33, 31]. In our model, steady-state heat conduction in the device (0 < x < L in Fig. 5) is governed by the following coupled heat diffusion equations,

$$\kappa_{coh-ph} \frac{d^2 T_{coh-ph}}{dx^2} - g(T_{coh-ph} - T_{inc-ph}) = 0,$$

$$\kappa_{inc-ph} \frac{d^2 T_{inc-ph}}{dx^2} - g(T_{inc-ph} - T_{coh-ph}) = 0,$$
(6a)

$$\kappa_{inc-ph} \frac{d^2 T_{inc-ph}}{dx^2} - g(T_{inc-ph} - T_{coh-ph}) = 0,$$
(6b)

in which Eq. 6a is for coherent phonons and Eq. 6b is for incoherent phonons in the device. In both equations,  $\kappa_{coh-ph}$  is the thermal conductivity of coherent phonons,  $\kappa_{inc-ph}$  is that of incoherent phonons, and g is the coupling factor between coherent and incoherent phonons, which quantifies how fast heat can transfer between these two heat conduction channels.

When coherent heat baths are used, i.e., the heat baths have the same  $\kappa_{coh-ph}$  and  $\kappa_{inc-ph}$  as those in the device, the effective thermal conductivity of the device is just

$$\kappa_{eff,coh-bath} = \kappa_{coh-ph} + \kappa_{inc-ph}. \tag{7}$$

In the case of incoherent heat baths as modeled in our NEMD simulations, we can assume that thermal transport in the heat baths is completely carried by the same incoherent phonons in the device, while coherent phonons that belong to the device do not exist in the baths. As detailed in Supplementary Information, we can show that the effective thermal conductivity of the device with incoherent baths is

$$\kappa_{eff,inc-bath} = \frac{\kappa_{coh-ph} + \kappa_{inc-ph}}{1 + \frac{\kappa_{coh-ph}}{\kappa_{inc-ph}} \frac{tanh(0.5\gamma L)}{0.5\gamma L}} = \frac{\kappa_{eff,coh-bath}}{1 + \frac{\kappa_{coh-ph}}{\kappa_{inc-ph}} \frac{tanh(0.5\gamma L)}{0.5\gamma L}},$$
(8)

where  $\gamma$  is defined as  $\gamma = \sqrt{g(\frac{1}{\kappa_{coh-ph}} + \frac{1}{\kappa_{inc-ph}})}$ .

Apparently, the effective thermal conductivity of the device with incoherent heat baths is always lower than that of the same device with coherent baths, i.e.,  $\kappa_{eff,inc-bath} < \kappa_{eff,coh-bath}$ . The reduced thermal transport in the incoherent system is caused by the bottleneck at the bath-device interfaces: on one hand, heat rejected by the hot bath can only first enter the incoherent phonon channel in the device and then transfer into the coherent phonon channel via incoherent-coherent phonon conversion; on the other hand, the heat carried by coherent phonons in the device has to transfer into incoherent phonons, again via incoherent-coherent phonon conversion, before it moves into the cold bath. These processes are manifested as nonequilibrium between coherent phonons and incoherent phonons at the bath-device interfaces, as illustrated in Fig. 5, which is similar to the case of electron-phonon nonequilibrium near metal-nonmetal interfaces reported in previous studies [32, 33, 31].

To further understand Eq. 8, we plot  $\kappa_{eff,coh-bath}/\kappa_{eff,inc-bath}$  as a function of the dimensionless device length  $\gamma L$  for a few representative cases. As shown in Fig. 6a,  $\kappa_{eff,inc-bath}$  is significantly lower than  $\kappa_{eff,coh-bath}$  when coherent phonons have a comparable or more contribution to thermal transport than incoherent phonons; the effect is more profound when the device is short, because the  $tanh(0.5\gamma L)/(0.5\gamma L)$  term in Eq. 8 monotonically decreases from 1 to infinitesimal when L varies from 0 to  $\infty$ . In particular, in the extreme case when the device is extremely short  $(\gamma L \to 0)$ , Eq. 8 predicts that  $\kappa_{eff,inc-bath} \to \kappa_{inc-ph}$ , which means negligible coherent phonon contribution to thermal transport through the device; in this case, replacing the incoherent baths with coherent ones can notably increase the effective thermal conductivity to  $\kappa_{eff,coh-bath} = \kappa_{coh-ph} + \kappa_{inc-ph}$  by fully exploiting the coherent phonon channel for thermal transport. In contrast, if coherent phonon contribution is negligible ( $\kappa_{coh-ph} \ll \kappa_{inc-ph}$ ) in the device material or when the device is very long ( $\gamma L \to \infty$ ), Eq. 8 reduces to  $\kappa_{eff,inc-bath} = \kappa_{coh-ph} + \kappa_{inc-ph}$ ; in this case, it does not matter whether coherent baths or incoherent ones are used, because  $\kappa_{eff,inc-bath}/\kappa_{eff,coh-bath} \approx 1$ , as shown in Fig. 6a.

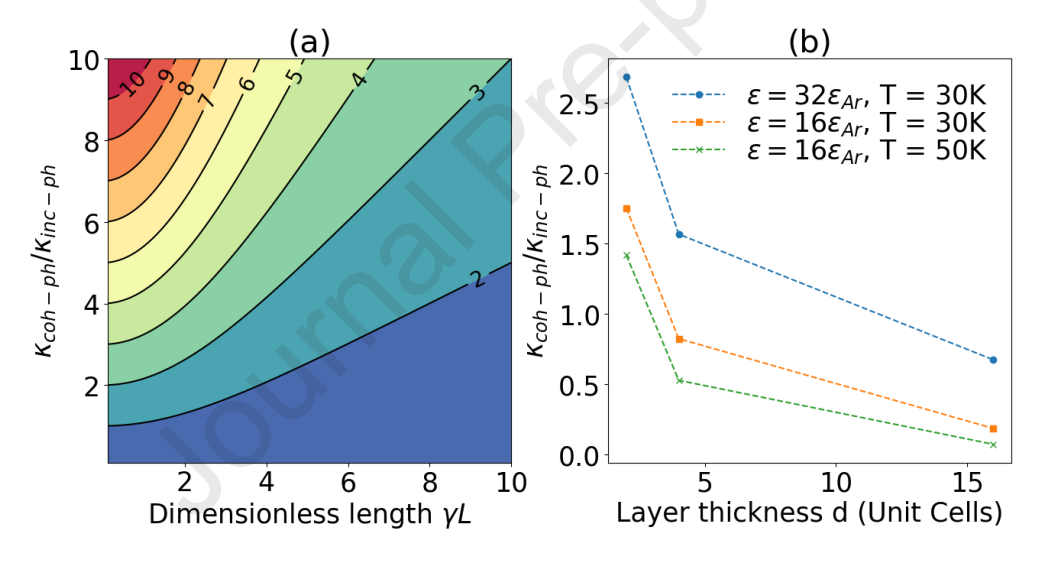


Figure 6: (a) 2D contour plot of  $\kappa_{eff,coh-bath}/\kappa_{eff,inc-bath}$  as a function of  $\kappa_{coh-ph}/\kappa_{inc-ph}$  and  $\gamma L$ , as predicted by Eq. 8. (b)  $\kappa_{coh-ph}/\kappa_{inc-ph}$  as a function of layer thickness of the superlattice deivce for different bond strength and temperature, which is obtained by fitting the coherent-incoherent phonon transport model to NEMD data.

Finally, we fit Eq. 8 to our NEMD results of  $\kappa_{eff,coh-bath}$  and  $\kappa_{eff,inc-bath}$  as a function of device length, of which the fitting details can be found in Supplementary Information. As shown in Fig. 6b, the contribution of coherent phonons increases when temperature decreases, when the layer thickness of the superlattice device decreases, or when the bond strength of the device material increases. This is consistent with the previously established conditions for observing strong phonon coherence in superlattices and other phononic crystals [38, 39, 37], which also explains why our NEMD simulations show stronger heat bath effect on  $\kappa_{eff}$  under those conditions.

#### 4. Conclusion

In summary, we demonstrated through rigorous molecular dynamics simulations that the lattice thermal conductivity of Lennard-Jones superlattice devices can be tailored by as much as 400% when switching between implementing incoherent heat baths and coherent baths. Spectral phonon transmission analysis reveals that there is significant phonon

nonequilibrium near the interface between incoherent heat baths and the device, while this phonon nonequilibrium is eliminated by implementing coherent heat baths. A coherent-incoherent phonon transport model is presented to further understand the heat bath effect on the overall thermal transport. Specifically, this analytical model reveals that when using incoherent baths, an extra thermal resistance will be introduced due to the nonequilibrium between coherent phonons and incoherent phonons, thus reducing the effective thermal conductivity. Our work provides a novel strategy to ex-situ and potentially widely tailor the lattice thermal transport in devices without modifying their composition or structure, which can be applied to thermal management of superlattice-like devices, e.g., densely packed nanotransistors and quantum cascade lasers, and the design of superlattice-based thermoelectric materials.

#### Credit author statement

**Tengfei Ma:** Conceptualization, Formal analysis, Software, Writing - Original Draft, Writing - Review & Editing. **Yan Wang:** Conceptualization, Formal analysis, Supervision, Writing - Original Draft, Writing - Review & Editing.

#### Data availability

The data supporting the findings of this work are available from the corresponding author upon reasonable request.

#### Acknowledgements

This work is supported by the NSF CAREER award (award number: 2047109) from the NSF-CBET Thermal Transport Processes Program. The authors thank the support of Research & Innovation and the Office of Information Technology at the University of Nevada, Reno for computing time on the Pronghorn High-Performance Computing Cluster.

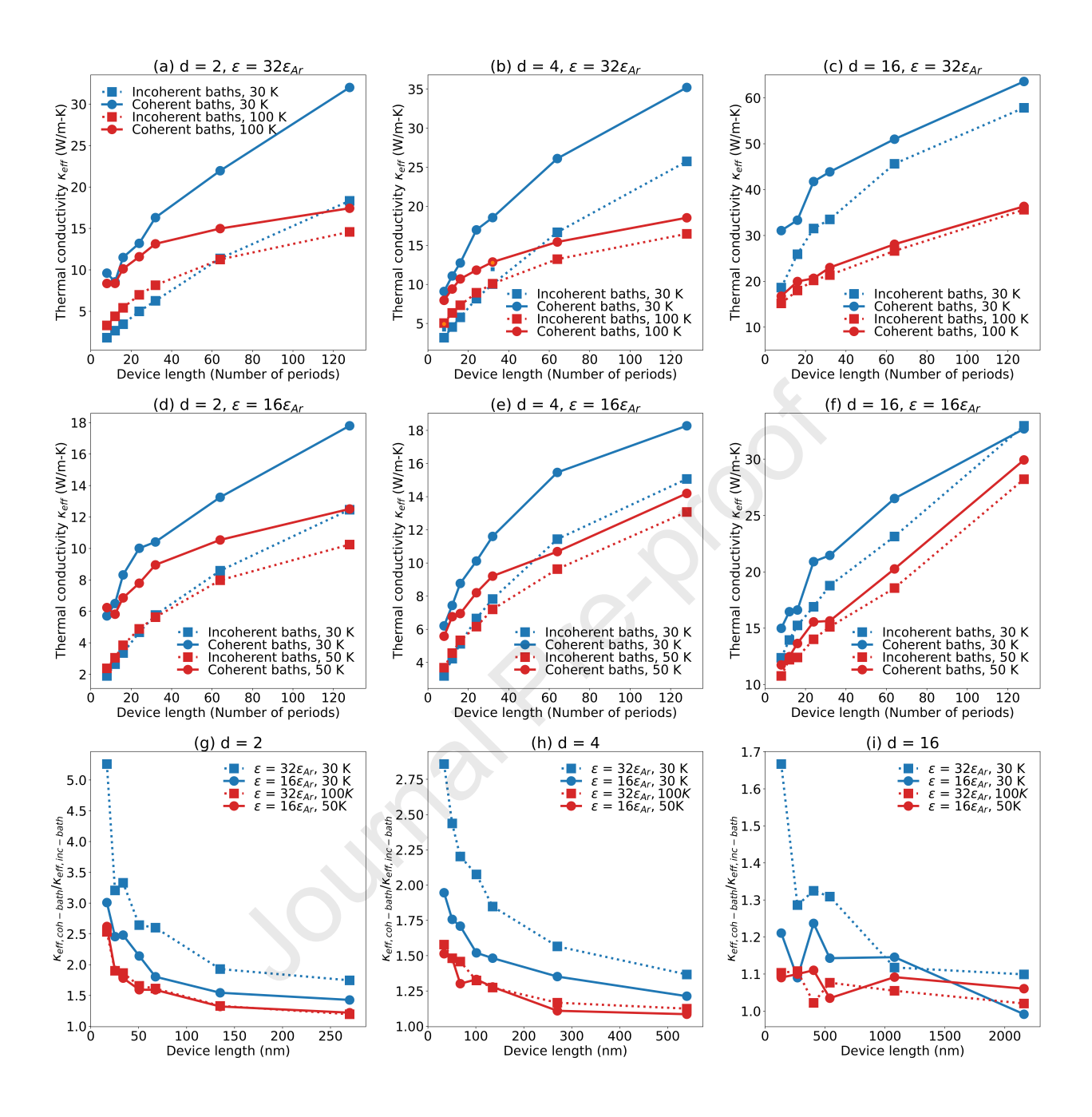
#### Appendix A. Supplementary data

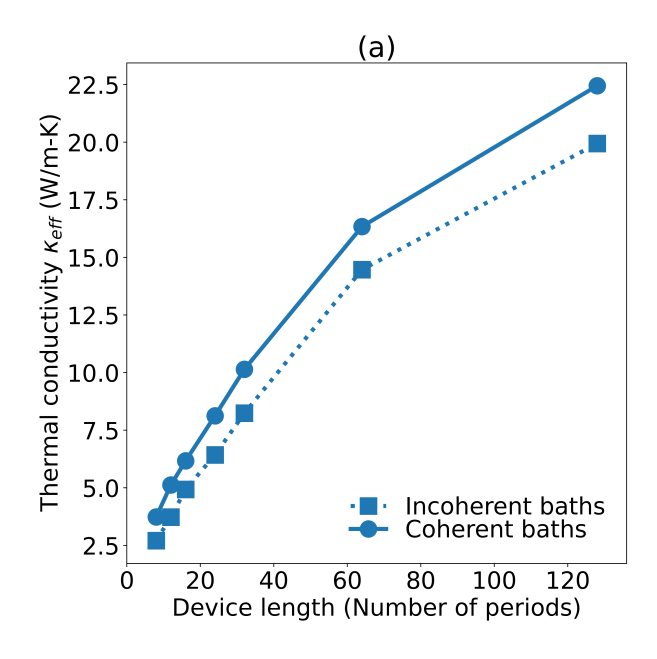
The following is the Supplementary data to this article.

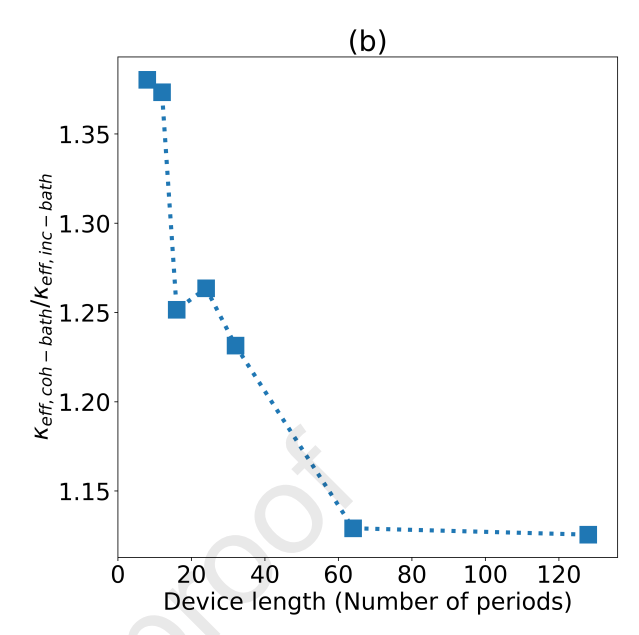
- Derivation of the effective thermal conductivity of a device with incoherent baths and fitting the coherent-incoherent phonon transport model to NEMD simulation data.
- [1] K. S. Novoselov, A. K. Geim, S. V. Morozov, D. Jiang, Y. Zhang, S. V. Dubonos, I. V. Grigorieva, and A. A. Firsov. Electric field effect in atomically thin carbon films. *Science*, 306(5696):666–669, 2004.
- [2] Jiuning Hu, Xiulin Ruan, and Yong P. Chen. Thermal conductivity and thermal rectification in graphene nanoribbons: A molecular dynamics study. *Nano Letters*, 9(7):2730–2735, 2009. PMID: 19499898.
- [3] Alexander A. Balandin, Suchismita Ghosh, Wenzhong Bao, Irene Calizo, Desalegne Teweldebrhan, Feng Miao, and Chun Ning Lau. Superior thermal conductivity of single-layer graphene. *Nano Letters*, 8(3):902–907, 2008. PMID: 18284217.
- [4] Jae Hun Seol, Insun Jo, Arden L. Moore, Lucas Lindsay, Zachary H. Aitken, Michael T. Pettes, Xuesong Li, Zhen Yao, Rui Huang, David Broido, Natalio Mingo, Rodney S. Ruoff, and Li Shi. Two-dimensional phonon transport in supported graphene. *Science*, 328(5975):213–216, 2010
- [5] Yan Wang, Ajit K. Vallabhaneni, Bo Qiu, and Xiulin Ruan. Two-dimensional thermal transport in graphene: A review of numerical modeling studies. *Nanoscale and Microscale Thermophysical Engineering*, 18(2):155–182, 2014.
- [6] Joon Sang Kang, Man Li, Huan Wu, Huuduy Nguyen, and Yongjie Hu. Experimental observation of high thermal conductivity in boron arsenide. Science, 361(6402):575–578, 2018.
- [7] Fei Tian, Bai Song, Xi Chen, Navaneetha K. Ravichandran, Yinchuan Lv, Ke Chen, Sean Sullivan, Jaehyun Kim, Yuanyuan Zhou, Te-Huan Liu, Miguel Goni, Zhiwei Ding, Jingying Sun, Geethal Amila Gamage Udalamatta Gamage, Haoran Sun, Hamidreza Ziyaee, Shuyuan Huyan, Liangzi Deng, Jianshi Zhou, Aaron J. Schmidt, Shuo Chen, Ching-Wu Chu, Pinshane Y. Huang, David Broido, Li Shi, Gang Chen, and Zhifeng Ren. Unusual high thermal conductivity in boron arsenide bulk crystals. *Science*, 361(6402):582–585, 2018.
- [8] Sheng Li, Qiye Zheng, Yinchuan Lv, Xiaoyuan Liu, Xiqu Wang, Pinshane Y. Huang, David G. Cahill, and Bing Lv. High thermal conductivity in cubic boron arsenide crystals. *Science*, 361(6402):579–581, 2018.
- [9] Fei Tian and Zhifeng Ren. High thermal conductivity in boron arsenide: From prediction to reality. *Angewandte Chemie International Edition*, 58(18):5824–5831, 2019.
- [10] Ke Chen, Bai Song, Navaneetha K. Ravichandran, Qiye Zheng, Xi Chen, Hwijong Lee, Haoran Sun, Sheng Li, Geethal Amila Gamage Udalamatta Gamage, Fei Tian, Zhiwei Ding, Qichen Song, Akash Rai, Hanlin Wu, Pawan Koirala, Aaron J. Schmidt, Kenji Watanabe, Bing Lv, Zhifeng Ren, Li Shi, David G. Cahill, Takashi Taniguchi, David Broido, and Gang Chen. Ultrahigh thermal conductivity in isotope-enriched cubic boron nitride. Science, 367(6477):555–559, 2020.

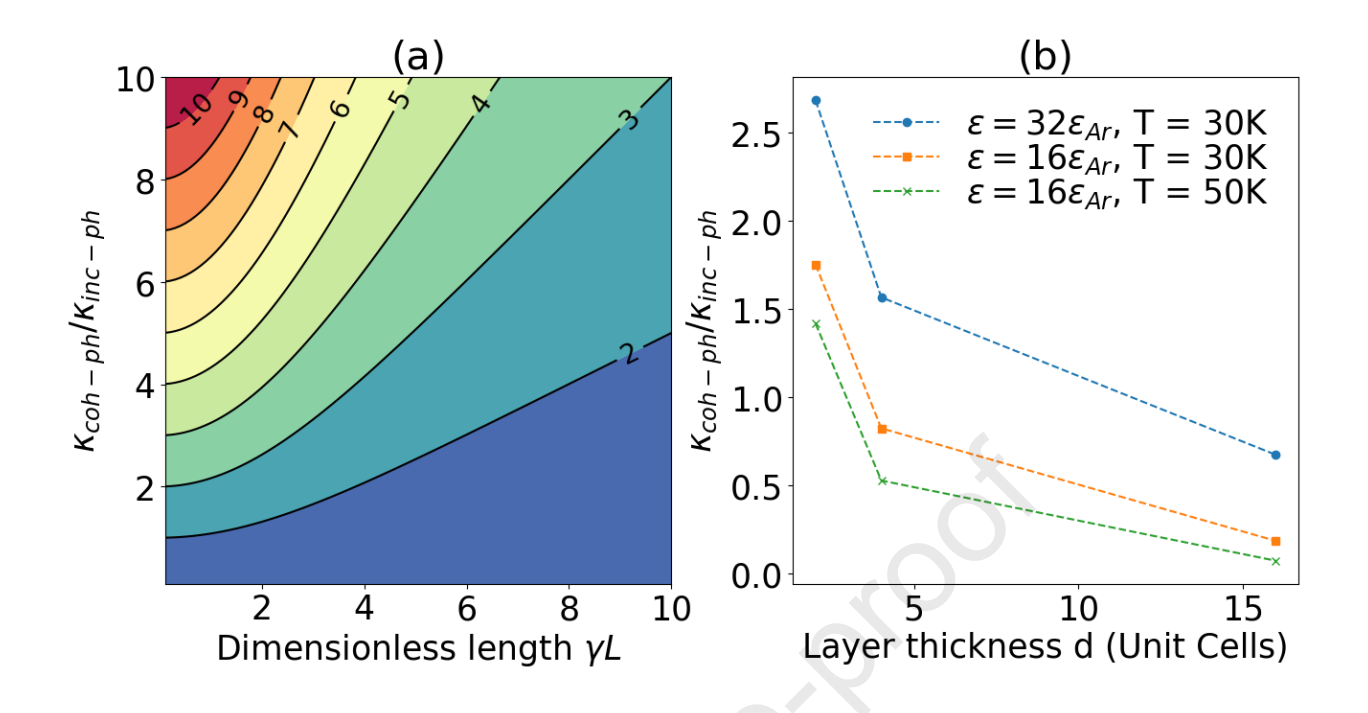
- [11] Pranay Chakraborty, Guoping Xiong, Lei Cao, and Yan Wang. Lattice thermal transport in superhard hexagonal diamond and wurtzite boron nitride: A comparative study with cubic diamond and cubic boron nitride. *Carbon*, 139:85 93, 2018.
- [12] Li-Dong Zhao, Shih-Han Lo, Yongsheng Zhang, Hui Sun, Gangjian Tan, Ctirad Uher, C. Wolverton, Vinayak P. Dravid, and Mercouri G. Kanatzidis. Ultralow thermal conductivity and high thermoelectric figure of merit in snse crystals. *Nature*, 508(7496):373–377, Apr 2014.
- [13] C. W. Li, J. Hong, A. F. May, D. Bansal, S. Chi, T. Hong, G. Ehlers, and O. Delaire. Orbitally driven giant phonon anharmonicity in snse. *Nature Physics*, 11(12):1063–1069, Dec 2015.
- [14] Cheng Chang, Minghui Wu, Dongsheng He, Yanling Pei, Chao-Feng Wu, Xuefeng Wu, Hulei Yu, Fangyuan Zhu, Kedong Wang, Yue Chen, Li Huang, Jing-Feng Li, Jiaqing He, and Li-Dong Zhao. 3d charge and 2d phonon transports leading to high out-of-plane zt in n-type snse crystals. *Science*, 360(6390):778–783, 2018.
- [15] Qian Xu, Jiawei Zhou, Te-Huan Liu, and Gang Chen. Effect of electron-phonon interaction on lattice thermal conductivity of sige alloys. *Applied Physics Letters*, 115(2):023903, 2019.
- [16] Allon I. Hochbaum, Renkun Chen, Raul Diaz Delgado, Wenjie Liang, Erik C. Garnett, Mark Najarian, Arun Majumdar, and Peidong Yang. Enhanced thermoelectric performance of rough silicon nanowires. *Nature*, 451(7175):163–167, Jan 2008.
- [17] Matthew R. Burton, Tianjun Liu, James McGettrick, Shahin Mehraban, Jenny Baker, Adam Pockett, Trystan Watson, Oliver Fenwick, and Matthew J. Carnie. Thin film tin selenide (snse) thermoelectric generators exhibiting ultralow thermal conductivity. *Advanced Materials*, 30(31):1801357, 2018.
- [18] Guofeng Xie, Zhifang Ju, Kuikui Zhou, Xiaolin Wei, Zhixin Guo, Yongqing Cai, and Gang Zhang. Ultra-low thermal conductivity of two-dimensional phononic crystals in the incoherent regime. *npj Computational Materials*, 4(1):21, Apr 2018.
- [19] B. Graczykowski, A. El Sachat, J. S. Reparaz, M. Sledzinska, M. R. Wagner, E. Chavez-Angel, Y. Wu, S. Volz, F. Alzina, and C. M. Sotomayor Torres. Thermal conductivity and air-mediated losses in periodic porous silicon membranes at high temperatures. *Nature Communications*, 8(1):415, Sep 2017.
- [20] Kouhei Takahashi, Masaki Fujikane, Yuxuan Liao, Makoto Kashiwagi, Takashi Kawasaki, Naoki Tambo, Shenghong Ju, Yasuyuki Naito, and Junichiro Shiomi. Elastic inhomogeneity and anomalous thermal transport in ultrafine si phononic crystals. Nano Energy, 71:104581, 2020.
- [21] Tengfei Ma, Cheng-Te Lin, and Yan Wang. The dimensionality effect on phonon localization in graphene/hexagonal boron nitride superlattices. 2D Materials, 7(3):035029, jun 2020.
- [22] Pranay Chakraborty, Yida Liu, Tengfei Ma, Xixi Guo, Lei Cao, Run Hu, and Yan Wang. Quenching thermal transport in aperiodic superlattices: A molecular dynamics and machine learning study. ACS Applied Materials & Interfaces, 12(7):8795–8804, 2020. PMID: 31994867.
- [23] Vikas Varshney, Soumya S. Patnaik, Ajit K. Roy, George Froudakis, and Barry L. Farmer. Modeling of thermal transport in pillared-graphene architectures. ACS Nano, 4(2):1153–1161, 2010. PMID: 20112924.
- [24] Jingjing Shi, Yalin Dong, Timothy Fisher, and Xiulin Ruan. Thermal transport across carbon nanotube-graphene covalent and van der waals junctions. *Journal of Applied Physics*, 118(4):044302, 2015.
- [25] Shin-Yi Yang, Kuo-Hsin Chang, Hsi-Wen Tien, Ying-Feng Lee, Shin-Ming Li, Yu-Sheng Wang, Jen-Yu Wang, Chen-Chi M. Ma, and Chi-Chang Hu. Design and tailoring of a hierarchical graphene-carbon nanotube architecture for supercapacitors. *J. Mater. Chem.*, 21:2374–2380, 2011.
- [26] Wen Dai, Tengfei Ma, Qingwei Yan, Jingyao Gao, Xue Tan, Le Lv, Hao Hou, Qiuping Wei, Jinhong Yu, Jianbo Wu, Yagang Yao, Shiyu Du, Rong Sun, Nan Jiang, Yan Wang, Jing Kong, Chingping Wong, Shigeo Maruyama, and Cheng-Te Lin. Metal-level thermally conductive yet soft graphene thermal interface materials. ACS Nano, 13(10):11561–11571, 2019. PMID: 31550125.
- [27] Shenghao Wu, Guoping Xiong, Huachao Yang, Biyao Gong, Yikuan Tian, Chenxuan Xu, Yan Wang, Timothy Fisher, Jianhua Yan, Kefa Cen, Tengfei Luo, Xin Tu, Zheng Bo, and Kostya (Ken) Ostrikov. Multifunctional solar waterways: Plasma-enabled self-cleaning nanoarchitectures for energy-efficient desalination. Advanced Energy Materials, 9(30):1901286, 2019.
- [28] Guangzhao Qin, Zhenzhen Qin, Sheng-Ying Yue, Qing-Bo Yan, and Ming Hu. External electric field driving the ultra-low thermal conductivity of silicene. *Nanoscale*, 9:7227–7234, 2017.
- [29] Sheng-Ying Yue, Runqing Yang, and Bolin Liao. Controlling thermal conductivity of two-dimensional materials via externally induced phonon-electron interaction. *Phys. Rev. B*, 100:115408, Sep 2019.
- [30] Chenhan Liu, Yunfei Chen, and Chris Dames. Electric-field-controlled thermal switch in ferroelectric materials using first-principles calculations and domain-wall engineering. *Phys. Rev. Applied*, 11:044002, Apr 2019.
- [31] Arun Majumdar and Pramod Reddy. Role of electronphonon coupling in thermal conductance of metalnonmetal interfaces. *Applied Physics Letters*, 84(23):4768–4770, 2004.
- [32] Yan Wang, Xiulin Ruan, and Ajit K. Roy. Two-temperature nonequilibrium molecular dynamics simulation of thermal transport across metal-nonmetal interfaces. *Phys. Rev. B*, 85:205311, May 2012.
- [33] Zexi Lu, Yan Wang, and Xiulin Ruan. Metal/dielectric thermal interfacial transport considering cross-interface electron-phonon coupling: Theory, two-temperature molecular dynamics, and thermal circuit. *Phys. Rev. B*, 93:064302, Feb 2016.
- [34] Ya Zhou and Alejandro Strachan. Phonon thermal transport outside of local equilibrium in nanowires via molecular dynamics. The Journal of Chemical Physics, 138(12):124704, 2013.
- [35] Jonathan Dunn, Edwin Antillon, Jesse Maassen, Mark Lundstrom, and Alejandro Strachan. Role of energy distribution in contacts on thermal transport in si: A molecular dynamics study. *Journal of Applied Physics*, 120(22):225112, 2016.
- [36] Zhen Li, Shiyun Xiong, Charles Sievers, Yue Hu, Zheyong Fan, Ning Wei, Hua Bao, Shunda Chen, Davide Donadio, and Tapio Ala-Nissila. Influence of thermostatting on nonequilibrium molecular dynamics simulations of heat conduction in solids. *The Journal of chemical physics*, 151(23):234105, 2019.
- [37] Yan Wang, Chongjie Gu, and Xiulin Ruan. Optimization of the random multilayer structure to break the random-alloy limit of thermal conductivity. *Applied Physics Letters*, 106(7):073104, 2015.
- [38] Yan Wang, Haoxiang Huang, and Xiulin Ruan. Decomposition of coherent and incoherent phonon conduction in superlattices and random multilayers. Phys. Rev. B, 90:165406, Oct 2014.
- [39] Pranay Chakraborty, Isaac Armstrong Chiu, Tengfei Ma, and Yan Wang. Complex temperature dependence of coherent and incoherent lattice thermal transport in superlattices. *Nanotechnology*, 32(6):065401, 2020.

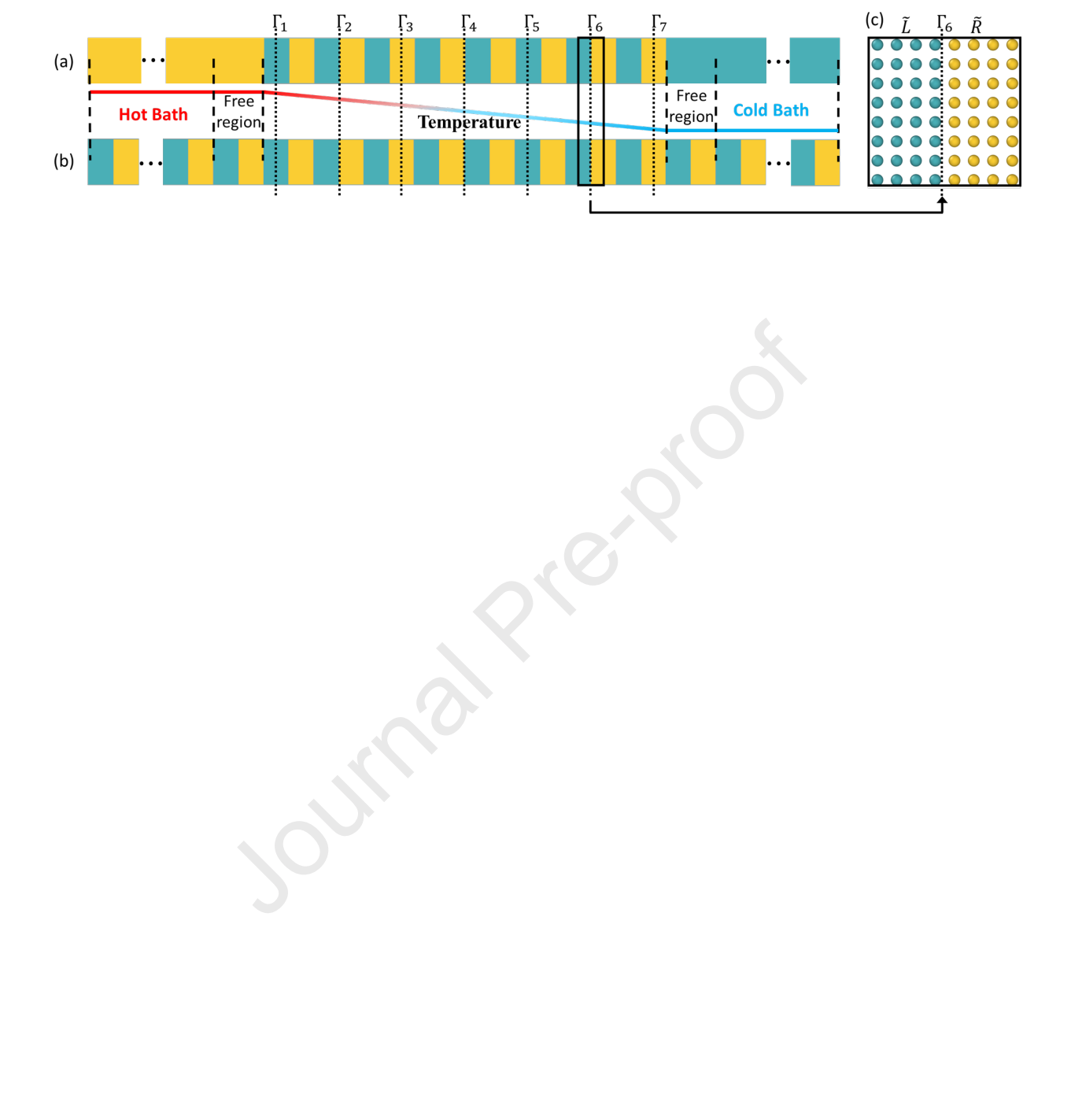
- [40] Pranay Chakraborty, Lei Cao, and Yan Wang. Ultralow lattice thermal conductivity of the random multilayer structure with lattice imperfections. *Scientific reports*, 7(1):1–8, 2017.
- [41] Bo Qiu, Gang Chen, and Zhiting Tian. Effects of aperiodicity and roughness on coherent heat conduction in superlattices. *Nanoscale and Microscale Thermophysical Engineering*, 19(4):272–278, 2015.
- [42] Taneli Juntunen, Osmo Vänskä, and Ilkka Tittonen. Anderson localization quenches thermal transport in aperiodic superlattices. *Phys. Rev. Lett.*, 122:105901, Mar 2019.
- [43] Samuel C. Huberman, Jason M. Larkin, Alan J. H. McGaughey, and Cristina H. Amon. Disruption of superlattice phonons by interfacial mixing. Phys. Rev. B, 88:155311, Oct 2013.
- [44] Martin Maldovan. Phonon wave interference and thermal bandgap materials. Nature Materials, 14(7):667-674, Jul 2015.
- [45] Maria N. Luckyanova, Jivtesh Garg, Keivan Esfarjani, Adam Jandl, Mayank T. Bulsara, Aaron J. Schmidt, Austin J. Minnich, Shuo Chen, Mildred S. Dresselhaus, Zhifeng Ren, Eugene A. Fitzgerald, and Gang Chen. Coherent phonon heat conduction in superlattices. *Science*, 338(6109):936–939, 2012.
- [46] Sergio Manzetti and Jean-Christophe P. Gabriel. Methods for dispersing carbon nanotubes for nanotechnology applications: liquid nanocrystals, suspensions, polyelectrolytes, colloids and organization control. *International Nano Letters*, 9(1):31–49, Mar 2019.
- [47] Y.-M. Lin, C. Dimitrakopoulos, K. A. Jenkins, D. B. Farmer, H.-Y. Chiu, A. Grill, and Ph. Avouris. 100-ghz transistors from wafer-scale epitaxial graphene. *Science*, 327(5966):662–662, 2010.
- [48] Mao-Lin Chen, Xingdan Sun, Hang Liu, Hanwen Wang, Qianbing Zhu, Shasha Wang, Haifeng Du, Baojuan Dong, Jing Zhang, Yun Sun, Song Qiu, Thomas Alava, Song Liu, Dong-Ming Sun, and Zheng Han. A finfet with one atomic layer channel. *Nature Communications*, 11(1):1205, Mar 2020.
- [49] D. Lei, K. H. Lee, Y. Huang, W. Wang, S. Masudy-Panah, S. Yadav, A. Kumar, Y. Dong, Y. Kang, S. Xu, Y. Wu, C. S. Tan, X. Gong, and Y. Yeo. Germanium-tin (gesn) p-channel fin field-effect transistor fabricated on a novel gesn-on-insulator substrate. *IEEE Transactions on Electron Devices*, 65(9):3754–3761, 2018.
- [50] M. Razeghi, Q. Y. Lu, N. Bandyopadhyay, W. Zhou, D. Heydari, Y. Bai, and S. Slivken. Quantum cascade lasers: from tool to product. Opt. Express, 23(7):8462–8475, Apr 2015.
- [51] Robert F. Curl, Federico Capasso, Claire Gmachl, Anatoliy A. Kosterev, Barry McManus, RafaÅ Lewicki, Michael Pusharsky, Gerard Wysocki, and Frank K. Tittel. Quantum cascade lasers in chemical physics. *Chemical Physics Letters*, 487(1):1 18, 2010.
- [52] Frank H Stillinger and Thomas A Weber. Computer simulation of local order in condensed phases of silicon. *Physical review B*, 31(8):5262, 1985
- [53] Kejian Ding and Hans C Andersen. Molecular-dynamics simulation of amorphous germanium. Physical Review B, 34(10):6987, 1986.
- [54] M Karimi, T Kaplan, M Mostoller, and DE Jesson. Ge segregation at si-ge (001) stepped surfaces. Physical Review B, 47(15):9931, 1993.
- [55] Steve Plimpton. Fast parallel algorithms for short-range molecular dynamics. Journal of computational physics, 117(1):1–19, 1995.
- [56] Aidan P Thompson, H Metin Aktulga, Richard Berger, Dan S Bolintineanu, W Michael Brown, Paul S Crozier, Pieter J in't Veld, Axel Kohlmeyer, Stan G Moore, Trung Dac Nguyen, et al. Lammps-a flexible simulation tool for particle-based materials modeling at the atomic, meso, and continuum scales. *Computer Physics Communications*, 271:108171, 2022.
- [57] Denis J Evans and Brad Lee Holian. The nose-hoover thermostat. The Journal of chemical physics, 83(8):4069-4074, 1985.
- [58] Kimmo Sääskilahti, Jani Oksanen, Jukka Tulkki, and Sebastian Volz. Role of anharmonic phonon scattering in the spectrally decomposed thermal conductance at planar interfaces. *Physical Review B*, 90(13):134312, 2014.
- [59] Kimmo Sääskilahti, Jani Oksanen, Sebastian Volz, and Jukka Tulkki. Frequency-dependent phonon mean free path in carbon nanotubes from nonequilibrium molecular dynamics. *Physical Review B*, 91(11):115426, 2015.
- [60] Tianli Feng, Wenjun Yao, Zuyuan Wang, Jingjing Shi, Chuang Li, Bingyang Cao, and Xiulin Ruan. Spectral analysis of nonequilibrium molecular dynamics: Spectral phonon temperature and local nonequilibrium in thin films and across interfaces. *Physical Review B*, 95(19):195202, 2017.
- [61] Yue Hu, Tianli Feng, Xiaokun Gu, Zheyong Fan, Xufeng Wang, Mark Lundstrom, Som S Shrestha, and Hua Bao. Unification of nonequilibrium molecular dynamics and the mode-resolved phonon boltzmann equation for thermal transport simulations. *Physical Review B*, 101(15):155308, 2020.

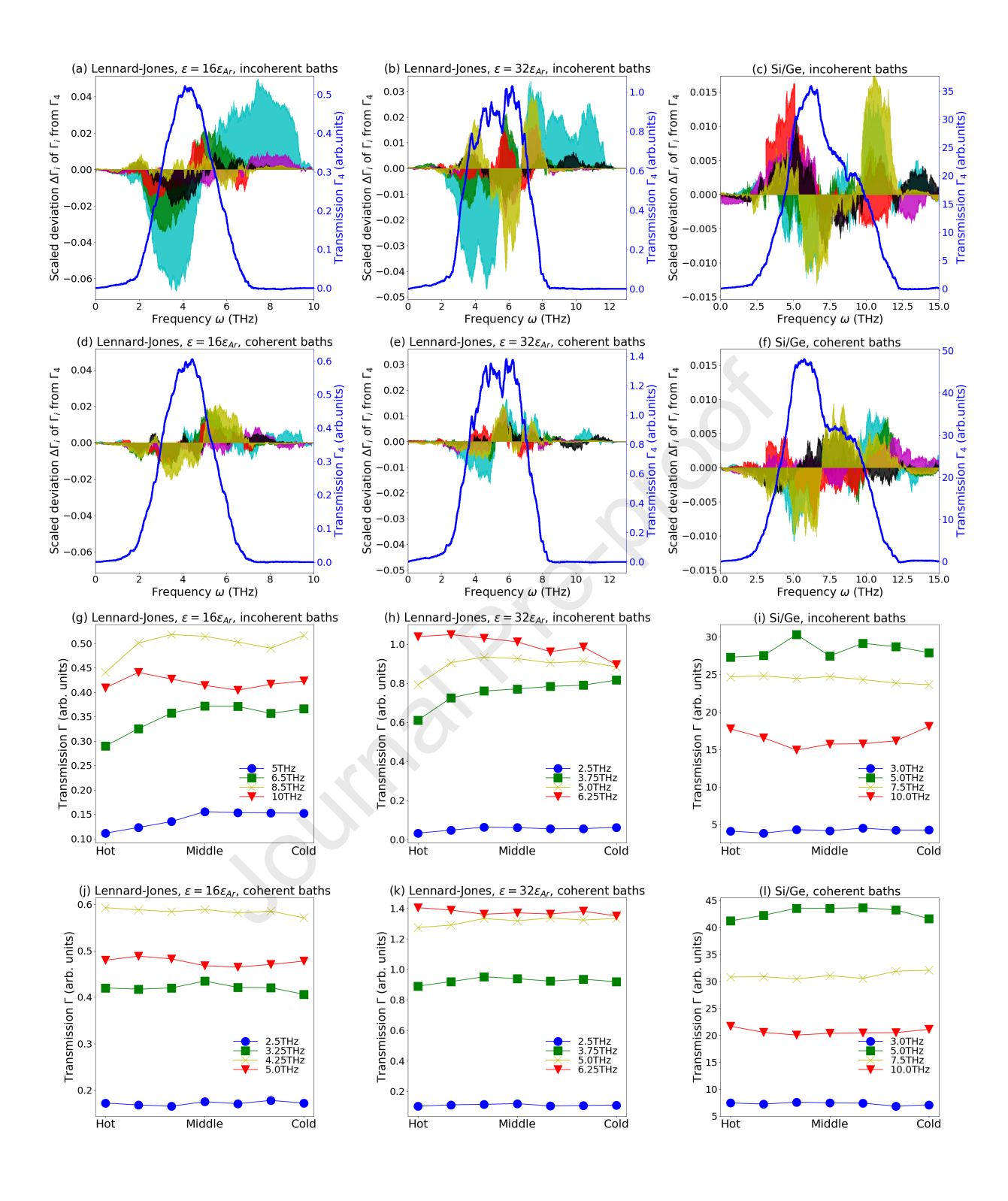


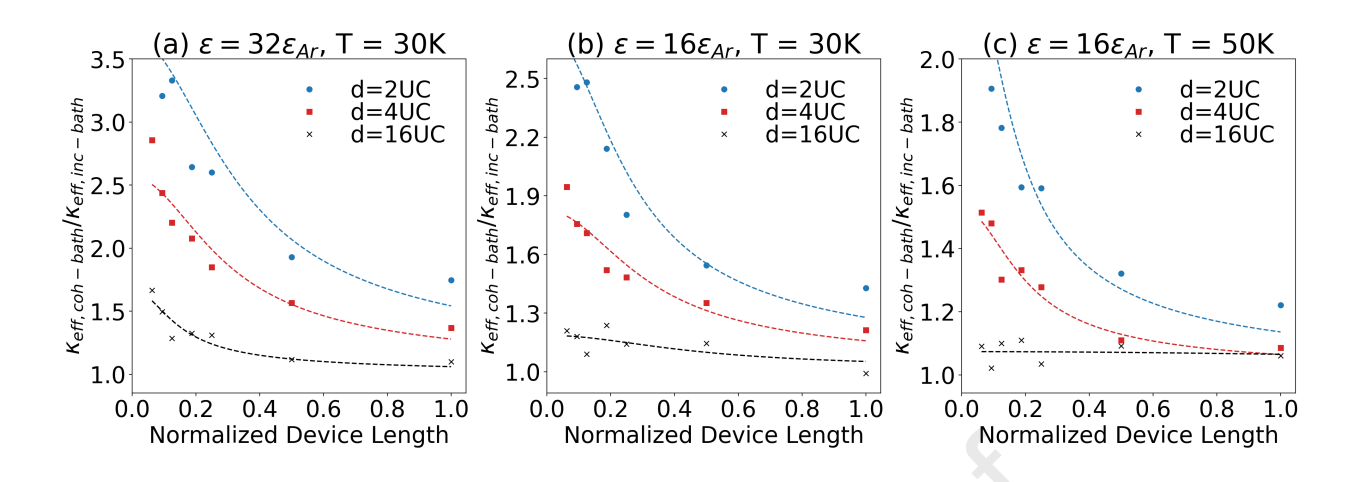












The highlights of our work are as follows:

- 1. We demonstrate the ex-situ modification of the thermal conductivity of nanodevices through the rational choice of heat baths.
- 2. We demonstrate that a superlattice device sandwiched between coherent heat baths, of which the phonon transmission spectra match with those of the device, can have significantly higher thermal conductivity than that of the same device attached to incoherent baths. The increase can be >400% for Lennard-Jones devices and >40% for room-temperature Si/Ge devices at room temperature.
- 3. Rigorous phonon transmission analysis reveals strong nonequilibrium between coherent phonons and incoherent phonons near the interface between the device and incoherent baths. In contrast, such nonequilibrium does not exist in devices with coherent baths.
- 4. We propose a coherent-incoherent phonon transport model, which clearly demonstrates that the coherent-incoherent phonon nonequilibrium leads to reduced thermal conductivity of the device.

Doc	laration	of into	rocte
Dec	iaraiion	OI INLE	71241

☑ The authors declare that they have no known competing financial interests or personal relationships that could have appeared to influence the work reported in this paper.
☐ The authors declare the following financial interests/personal relationships which may be considered as potential competing interests: